Modelling of TiO_2-Perovskite Interface

Agustín Bou Català

Treball fi de màster

Juliol 2017

Aquest treball “Modelling of TiO_2-Perovskite Interface” es presenta com a treball fi de màster d’Agustín Bou Català dirigit pel Professor Juan Bisquert el dia 03/07/17. El treball ha donat lloc a la publicació de l’article:

Ghahremanirad, E.; Bou, A.; Olyaee, S.; Bisquert, J. Inductive loop in the impedance response of perovskite solar cells explained by surface polarization model. *J. Phys. Chem. Lett.* **2017,** *8,* 1402-1406.

La comissió està formada per Francisco Fabregat Santiago, Germà Garcia Belmonte i Iván Mora Seró.

Content

Abstract

Perovskite-TiO_2 interface has become crucial for the operation of perovskite solar cell devices. In this work, we show an equivalent circuit for the impedance spectroscopy response of these devices that has been calculated for a previous model that was developed for explaining the accumulation in the perovskite-TiO_2 interface. This circuit explains unique behaviors such as the inductive loop and the negative capacitance. To get more insight, we show the results from the modelling of this interface by solving the Poisson equations on both sides for the case of accumulation.

1. Introduction

The question of energy has become a central topic all around the globe due to its increasing demand and the problems caused by some of the ways we use to obtain this amount of energy. There is a widely extended belief that important changes have to be carried out with the objective of a cleaner and sustainable way of obtaining power. From one side, the growth in energy use is being balanced in part by the important progress made in increasing the efficiency in most of the objects or machines that we use on a daily basis. From the other side, the advances in new forms of "green" energies help the accomplishment of such goals of the use of cleaner carbon-free energies.

Here, we focus on the challenging field of getting power from new and clean sources. It is a fact that the majority (more than 80%) of the world's power comes from fossil fuels, such as coal, oil and natural gas.[1] Despite being greatly powerful, these sources lack of a continue supply and will eventually be exhausted. Moreover, the damage caused to the atmosphere and the air we breathe by exploiting them in thermal plants and vehicles has been demonstrated to be dangerous, with fatal consequences.[2] This explains the importance of the development of the new "green" energies, i.e. wind, solar and wave power, which have started to be set up and expanded at many countries in the recent years.[1]

The main topic of this work is related with solar power. The amount of energy that arrives the Earth from the Sun is enormously large compared to the energy consumption of humankind.[3] Combined with the fact that its exploitation produces no harm or drawback makes solar energy a great candidate for sustainable power supply.[4] That is the reason why there has already been a lot of research in the development of photovoltaics. Crystalline silicon has developed for more than 60 years[5] and it is nowadays the industry leader[6] due to its stability, high efficiency and low cost. Nevertheless, other technologies have been developed which increase the versatility of the field in the search of a variety of applications. Some typical examples are CdTe and CIGS thin film solar cells,[7] dye-sensitized solar cells[8] and organic solar cells.[9] But the latest technology to emerge has been the perovskite solar cells. Its irruption in the field has extended so quickly due to its fast increase of solar to electricity power conversion efficiency to more than 20%.[10]

Perovskite is used to denominate a family of materials whose general formula is ABX_3. In the case of our devices used for photovoltaic conversion the A corresponds a methylammonium molecule, the B is for a Pb atom and the X is for a halide, usually Iodide, these are the so-called hybrid organic-inorganic halide perovskites. These perovskites have a number of properties that make them real candidates for the new generation of solar cells. These properties are, for example, good absorption, fast transport, low non-radiative recombination and a suitable gap that can be taylored to absorb the visible light,[11] which makes it ideal for tandem cells. For the development of these devices, an accurate design and configuration are essential. This configuration regards the active or absorber layer, and the electron and hole selective contacts, as well as the interfaces. In this work, the interface between the perovskite and the TiO_2 as electron selective contact are key point of study, due to its importance in the performance of the device.

Investigating and understanding the physical processes in the bulk and the interfacial layers are main topics in perovskite solar cells for the control of the device quality and for the design of new applications. Impedance Spectroscopy (IS) is a very useful tool to characterize physical processes in solar cell devices and it has been applied extensively in the perovskite solar cells. Here, it will be the main technique considered to model the TiO_2-perovskite interface. Many reports have presented the suggestion of equivalent circuits, the comparison with previous solar cell systems, and the analysis of the resulting processes.[12-15] Further recognition of the ionic drift in the lead halide perovskite material introduced the need to discuss the mixed conduction and modification of the interfaces.[16-18]

Very interesting and unique behaviours that have been shown in the literature in the impedance response plot are the negative capacitance[19-20] and also an inductive loop.[16, 21] The negative capacitance at low frequency is a familiar feature on hybrid organic-inorganic solar cells,[22] but explaining the specific microscopic origin of such feature is traditionally rather challenging. An inductive loop is a middle-frequency range feature that in some cases goes to the negative capacitance as well. This loop has been well established in perovskite solar cells,[16, 21] but the origin and significance of this loop for the solar cell operation is not clear at all. The inductance simply appears as a necessary feature in the equivalent circuits to fit the experimental data without a clear explanation of the physical process that creates it.

In this work, an explanation of the origin of the frequently observed impedance loops is provided based on a recently proposed surface polarization model[23] and without further assumptions. We also show the adequate description of experimental IS data by this model that is simply computed from the previously proposed equations, thus providing support to the model and additional insight to the kinetic properties of the perovskite solar cell.

2. The surface polarization model

From the very beginning of perovskite solar cells research, a dynamic hysteresis has been found in the current density-voltage (j-V) curves.[19, 24-25] This consists in a deviation of the shape of the stationary response depending on the previous and the initial conditions of the measurements, as well as the way the measurements are carried. Its explanation is very challenging due to the wide variety of phenomenology involving it. In this work, we take a model previously proposed for the explanation of the dynamic hysteresis and we make the impedance calculations to propose an equivalent circuit for the response of the IS measurements. We also describe the observable features that the model includes.

The Surface Polarization Model (SPM) is supported by reported evidence of capacitance results for the surface polarization.[16, 26-30] This surface polarization refers to a strong electronic charging in the TiO_2-perovskite when forward biasing is applied, which is assisted by the presence of mobile ions coming to the interface.[18, 29-31] The main support for this model comes from IS measurements, looking at capacitance versus frequency plots, where we can observe a large low-frequency capacitance that has been associated with the ionic polarization at the interface.[31-32] Zarazua et al. suggested an interpretation for this large capacitance, associating it to the accumulation of holes at the interface.[29] From that, they proposed the upward band bending at the electron contact. But the accumulation of holes is not enough to describe the long-time transients that are observed in open-circuit voltage decay,[30] since these electronic interfacial states can't produce these slow kinetics effects. For this reason, here, both holes and ionic accumulation is considered for the model. It must be said that hysteresis practically disappears when using fullerene[33] instead of TiO_2 contacts, what makes the interface effects more evident of causing hysteresis.

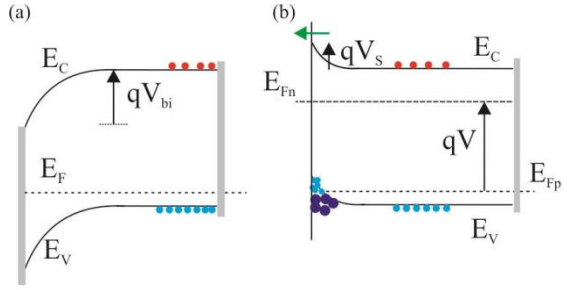

Fig. 1. The energy diagram of a perovskite solar cell in which electron selective contact locates at the left and hole selective contact locates at the right side. (a) Equilibrium condition in the dark. (b) Open circuit under illumination condition. E_c, E_v: Edges of conduction and valence bands. E_F: Fermi Level. E_{Fn}, E_{Fp}: Quasi-Fermi level of electrons and holes. V: External voltage of the contacts. V_{bi}: The constant built-in voltage. V_s: The variable surface polarization voltage. Indicated in (b) are the accumulation of holes and cations, and the tunnelling of electrons across the surface barrier.

The surface polarization model[23] starts from this upward band bending assumption which creates a surface voltage in the perovskite solar cell. This voltage is a consequence of the accumulation of charge at both sides of the interface between the perovskite and the TiO_2 electron selective contact as indicated in Fig. 1. The band bending structure at forward bias voltage in Fig. 1 has been established from detailed simulations.[30] V is the external voltage at the contacts and V_s is an internal surface polarization voltage associated to the accumulation layer of holes assisted by positive ion charge that results from the ionic displacement, and compensated by electrons in the contact layer side of the interface. The excess charge density of holes at the interface is

$$Q_s = qp_s = Q_{s0} e^{qV_s/\gamma k_B T} \tag{1}$$

as a function of surface hole density, p_s, the elementary electrical charge, q, the thermal energy $k_B T$, and the equilibrium surface charge Q_{s0}. The capacitance associated to surface charging is

$$C_1 = \frac{dQ_s}{dV_s} = \frac{qQ_{s0}}{\gamma k_B T} e^{qV_s/\gamma k_B T} \tag{2}$$

The exponent γ takes the value of 2 in the case of purely electronic accumulation capacitance.[29] At equilibrium condition at a given voltage V,

$$V_s = V - V_{bi} \tag{3}$$

where V_{bi} is a built-in voltage. The presence of ions at the interface implies that the build-up and recovery of the equilibrium distribution is severely impeded by the rate of ion migration, governed by the already mentioned slow kinetics.[30] Thus the internal voltage V_s cannot follow the external voltage instantaneously but reacts slowly to achieve the condition imposed by V. This characteristic behaviour has been described by a relaxation equation of the type[23]

$$\frac{dV_s}{dt} = -\frac{V_s - (V - V_{bi})}{\tau_{kin}} \tag{4}$$

where the relaxation kinetic constant τ_{kin} is determined by the rapidity of ion displacement at the specified illumination and temperature.

Next, we establish the standard photovoltaic properties of the solar cell, in order to form a diode equation. Recombination current at the surface of the cell depends on electron and hole concentration[34]

$$j_{rec} = k_{rec} n Q_s \tag{5}$$

with a recombination rate constant k_{rec}. The bulk electron density is $n = n_0 \exp(qV / \beta k_B T)$, hence the recombination current in transient condition is

$$j_{rec} = j_{rec0} e^{qV_{bi}/\gamma k_B T} e^{q(V_s/\gamma + V/\beta)/k_B T} \tag{6}$$

where β is an ideality parameter taken here $\beta = 1$ and j_{rec0} is the recombination parameter. The steady state solution of the recombination equation is obtained by imposing the equilibrium value of surface voltage in Eq. 3:

$$\bar{j}_{rec} = \bar{j}_{rec0} e^{q\bar{V}/mk_B T} \tag{7}$$

where $m = \gamma\beta/(\gamma + \beta)$. To complete the SPM in a transient situation the extracted current is composed by the photocurrent j_{ph}, minus the recombination current, and the current of the excess electrons extracted from the contact. Hence

$$j = j_{ph} - j_{rec0} e^{q(V_s/\gamma + V/\beta + V_{bi}/\gamma)/k_B T} + C_1 \frac{dV_s}{dt} \tag{8}$$

3. Impedance model

For calculating the IS response of the previously presented SPM, a small ac perturbation (denoted by tilde) of angular frequency ω is applied to the voltage, added to the steady state characteristic (indicated by overbar). By taking the Laplace transform, the small amplitude current is

$$\hat{j} = \bar{j}_{rec}\left(\frac{q\hat{V}_s}{\gamma k_B T} + \frac{q\hat{V}}{\beta k_B T}\right) + i\omega C_1 \hat{V}_s \tag{9}$$

The small perturbation surface polarization voltage is calculated by taking a Laplace transform of the Eq. 4:

$$\hat{V}_s = \frac{\hat{V}}{1 + i\omega\tau_{kin}} \tag{10}$$

By substituting Eq. 10 in Eq. 9, the following expression for the ac impedance is obtained:

$$Z = \frac{\hat{V}}{\hat{j}} = \left[i\omega C_d + \frac{1}{R_L + i\omega L} + \frac{1}{R_{rec}} + \frac{1}{R_c - i\dfrac{1}{\omega C_1}} \right]^{-1} \tag{11}$$

where the equivalent circuit elements have the following values in terms of model parameters:

$$\begin{aligned} R_{rec} &= \frac{\beta k_B T}{q\bar{j}_{rec}} \\ R_L &= \frac{\gamma k_B T}{q\bar{j}_{rec}} \\ L &= \tau_{kin} R_L \\ R_C &= \frac{b\tau_{kin}}{C_1} \end{aligned} \tag{12}$$

A representation of the model of Eq. (11) as an equivalent circuit is shown in Fig. 2. In this circuit, R_s is a series resistance and R_{rec} is a recombination resistance that is inversely related to the steady state recombination current density $\bar{j}_{rec}$. The capacitance C_d is added to represent the *dielectric* bulk (or surface) processes that usually occur at high frequency.[16] R_L is the series resistance with the inductance L and both of them are

inversely proportional to $\bar{j}_{rec}$. The inductance L has a direct dependence on the τ_{kin} . R_C is the series resistance with the capacitance C_1 and it is also directly dependent on the τ_{kin} and an additional parameter b that is justified below.

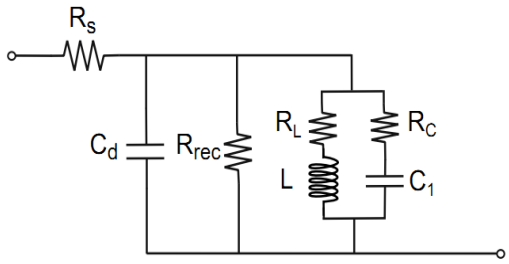

Fig. 2. Equivalent circuit obtained by applying a small ac perturbation. In this circuit, R_s is the series resistance, C_d is the dielectric capacitance, R_{rec} is the recombination resistance, R_L is the series resistance with the inductance L and R_C is the series resistance with the surface charging capacitance C_1.

The physical interpretation of the circuit is the following. The parallel $R_{rec} - C_d$ combination is the standard ac circuit for a solar cell governed by recombination. For a perovskite solar cell the recombination may fluctuate from bulk to surface dominated process depending on specific conditions.[35] In parallel to the usual solar cell elements, there are two parallel lines that correspond to the accumulation and extraction of charge at the surface. First, the line $R_C - C_1$ is the charging and discharging of the surface accumulation capacitance controlled by the kinetic relaxation time τ_{kin} . The second line $R_L - L$ is an additional nonstandard process. This is a remarkable feature of the model that follows directly from Eq. (4). As we explained before, there is a delay for the surface charging with respect to external voltage because of the ions movement that governs the equilibration of the interface controlled by the kinetic relaxation constant τ_{kin}. This delay time is the reason of the inductive line in the equivalent circuit.

4. Interpretation of impedance spectra

In Fig. 3 we show the characteristic spectra associated to the impedance model. We also indicate the values of low and high frequency resistances. At the low frequency region, the inductance and the capacitances act as a short circuit and open-circuit, respectively. Therefore, the value of the Z' at the end point of the spectra is given by the series-parallel combination $R_{lf} = R_s + R_{rec} \| R_L$. At the high frequency region, $R_{hf} = R_s$.

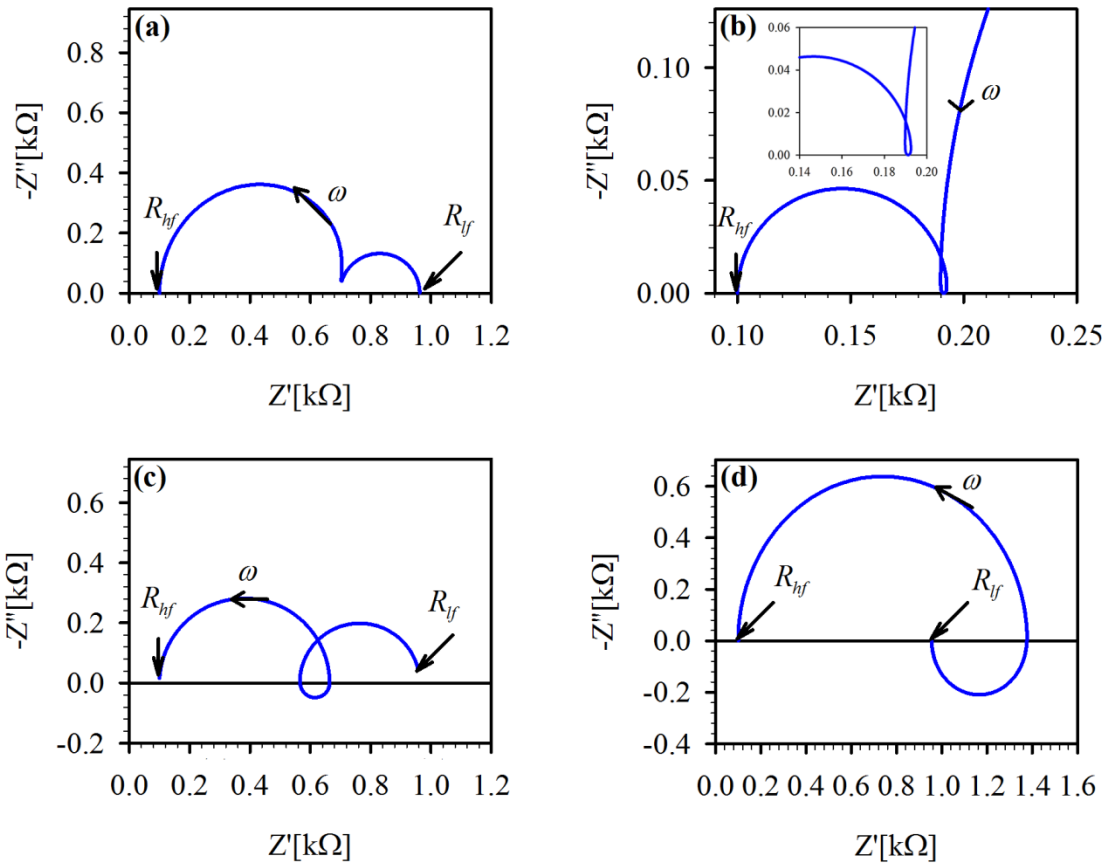

Fig. 3. Typical complex plane impedance plots obtained for different values of kinetic relaxation constant τ_{kin} at different applied biases for the following values of $V_{bi} = 0.5V$, $V_{oc} = 0.95V$, $\varepsilon = 30$, $j_{ph} = 20 mA cm^{-2}$, $\gamma = 2$, $\beta = 1$, $k_B T / q = 0.026eV$, $Area = 0.1\ cm^2$ and the following values for the resistances and capacitances: $R_{hf} = R_s = 100 \Omega cm^2$, $R_{lf} = R_{rec} \| R_L = 96.3 \Omega cm^2$, $C_{bulk} = 10^{-5}\ F\ cm^{-2}$, and the other values for (a) $\tau_{kin} = 0.1s$, $L = 25.88 H\ cm^{-2}$, $R_C = 200 \Omega cm^2$, $C_1 = 5 \times 10^{-4}\ F\ cm^{-2}$, (b) $\tau_{kin} = 1\ s$, $L = 258.8\ H\ cm^{-2}$, $R_C = 10\ \Omega cm^2$, $C_1 = 0.1\ F\ cm^{-2}$ (inset shows the zoomed-in view of the positive loop), (c) $\tau_{kin} = 10s$, $L = 2588 H\ cm^{-2}$, $R_C = 100 \Omega cm^2$, $C_1 = 0.1\ F\ cm^{-2}$ and (d) $\tau_{kin} = 100s$, $L = 25880 H\ cm^{-2}$, $R_C = 10 k\Omega cm^2$, $C_1 = 0.01\ F\ cm^{-2}$.

The first spectrum (a), shows two positive arcs. The combination of resistances R_{rec} and R_L determines the diameter of the arcs. This type of spectra has been found in many works of IS of the perovskite solar cells, and it is often observed that the two arcs have similar width and vary in a coupled way when the voltage or illumination are changed.[34] We note that in the model R_{rec} and R_L show a similar voltage dependence, which may explain the unisonous variation of the distinct low frequency arcs frequently observed in the literature.

By increasing the value of τ_{kin} and the capacitance C_1, a positive inductive loop appears in the impedance spectrum (b). The inductance becomes more dominant for larger values of the kinetic relaxation constant. Then, the loop becomes bigger and crosses the axis entering negative capacitance values (c). When the kinetic relaxation constant is increased to large values (here 100 s), the low frequency arc goes into negative capacitance (d), a behaviour that is well documented.[20] These two significant impedance spectra, i.e. the inductive loop and the negative capacitance at low frequency, are explained theoretically for the first time.

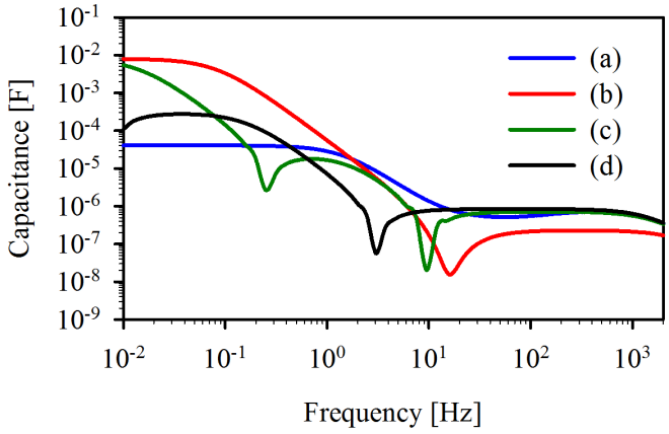

Fig. 4. The capacitance-frequency ($C-f$) spectra are calculated for the spectra of Fig. 3. The 'blue', 'red', 'green', and 'black' curves show the C-F plot of the Fig. 3 (a), (b), (c) and (d), respectively.

Fig. 4 shows the capacitance-frequency ($C-f$) plots for the complex impedance spectra of Fig. 3 where the real part of the capacitance is taken from the complex capacitance $C=1/i\omega Z$.[36] The low frequency part of the curves corresponds to the capacitance C_1 and the high frequency part shows the dielectric capacitance. In the cases with negative capacitance the undershoots in the curve correspond to the transition to negative capacitance in Fig. 3. Also, an undershoot appears in plot (b) at frequencies that the positive loop gets very close to the frequency axis.

In order to establish the suitability of the model for the description of experimental results, we have analyzed previously reported impedance spectra.[21] The spectra have been measured in perovskite solar cells with special electron selective consisting of a periodic multilayered structure that magnifies the effects of the interface. The sequential deposition of SiO_2 and TiO_2 mesoporous layers forces multiple electron injection processes which cause very large loop features in the impedance plots.

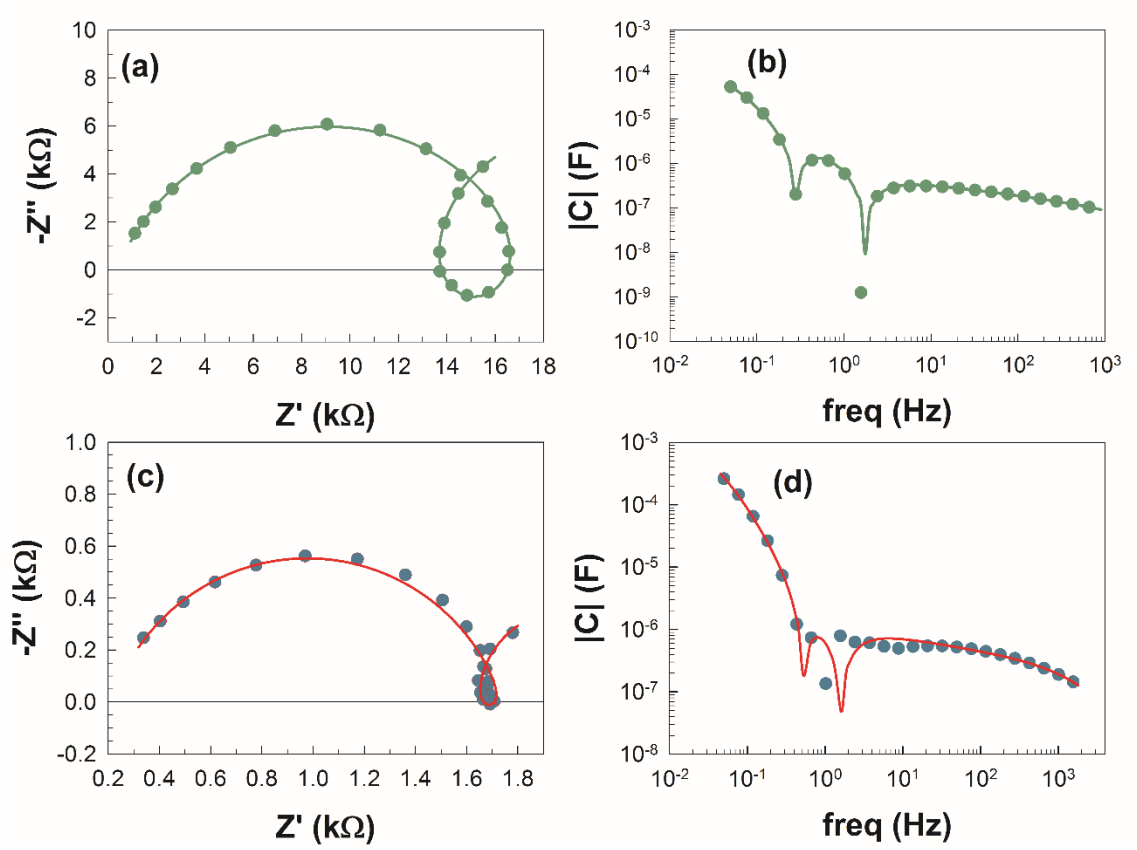

Fig. 5. Impedance and capacitance-frequency ($C-f$) spectra obtained under illumination and with an applied bias of 0.7 V. (a) and (c) show the complex impedance plots of two different perovskite samples S1 (green) and S2 (red). (b) and (d) show their ($C-f$) plots, respectively. The circles represent the experimental points, while solid lines are the fitting curves using the equivalent circuit. For (a) $R_s = 33.8\ \Omega\cdot cm^2$, $R_{rec} = 4700\ \Omega\cdot cm^2$, $C_d = 1.11\times10^{-5}\ F\cdot cm^{-2}$, $R_L = 4350\ \Omega\cdot cm^2$, $L = 123\ kH\cdot cm^{-2}$, $R_C = 2460\ \Omega\cdot cm^2$, $C_1 = 1.38\times10^{-3}\ F\cdot cm^{-2}$. For (b) $R_s = 19.6\ \Omega\cdot cm^2$, $R_{rec} = 219\ \Omega\cdot cm^2$, $C_d = 2.54\times10^{-5}\ F\cdot cm^{-2}$, $R_L = 2\ k\Omega\cdot cm^2$, $L = 45\ kH\cdot cm^{-2}$, $R_C = 390\ \Omega\cdot cm^2$, $C_1 = 0.011\ F\cdot cm^{-2}$.

In Fig. 5 we show two characteristic spectra, and the fitting with the equivalent circuit of the SPM provides the results indicated in Table 1. Values of $\bar{j}_{rec}$ and C_1 are of the same order of magnitude in both cases. Values of τ_{kin} are similar with those previously obtained in the fitting of the dynamic hysteresis of the $j-V$ curves in our previous work.[23] We take the agreement of very different experimental methods as encouraging support of the SPM based on Eq. (4).

The SPM generates the equivalent circuit of Fig. 2 with the parameter b in Eq. 12 having a value 1. However, we note in Table 1 that the experimental value of the parameter b is around 0.1-0.2 in both cases. The interpretation of this finding is the

following. The equivalent circuit is generated from the theory with a restricted number of parameters of the model, which are essentially three, namely the recombination current density $\bar{j}_{rec}$, the kinetic relaxation constant τ_{kin} and $C_{s0} = qQ_{s0}/k_BT$. It appears that the equivalent circuit describes well the experimental data, but the additional parameter b is needed to generate a richer set of spectra. This is far from surprising, as the previously formulated SPM incorporates a kinetic delay of charge at the surface but not the energy loss process across the interface such as electron transfer by tunneling suggested in Fig. 1.[37] The departure of b from the value 1 indicates that the spectra possess additional physical characteristics that need to be described by a more general model. We suggest that a resistive process for charge transfer across the interface may be needed, in agreement with the usual observation of a major decrease of photocurrent in the presence of poorer contacts, that causes a substantial decrease of solar cell performance.[16]

Sample	$\bar{j}_{rec}(mA/cm^2)$	$C_d(F\,cm^{-2})$	$C_1(F\,cm^{-2})$	$\tau_{kin}(s)$	b
S_1	0.012	1.11×10^{-5}	1.38×10^{-3}	28.2	0.12
S_2	0.027	2.54×10^{-5}	0.011	23	0.19

Table 1. Values calculated from the fittings of the IS data of two perovskite solar cells[21] to the equivalent circuit of Fig. 2.

In summary, we have developed new implications from a surface polarization model that assumes a kinetic delay of the state of the interface by slow build up of ionic charge. Previously the model was used to describe dynamic hysteresis in the voltage sweep curves, and here we found the characteristics of impedance spectroscopy, which bring about two conclusions. First, due to the peculiar kinetic delay, the surface processes produce a highly structured spectral shape consisting of at least two impedance arcs, that will vary in coordination, since they reflect unique underlying characteristics. The second conclusion is the appearance of inductive loops, either positive or negative capacitance, that have been widely observed previously in the experimental reports. We show that the loops contain important kinetic information about the behaviour of the interfaces of perovskite solar cells. The fitting of data suggest that the experimental response is even richer than that covered by our model, indicating the need for extensive studies in order to clarify the complex behaviour of the perovskite solar cell.

5. Modelling of the electric potential distribution at the interface

From this initial model for the Impedance Spectroscopy and its fitting results from real spectra, we have seen that there is still more information in them, due to phenomena still not taken into account in the model. Investigating the situation, we can observe that the huge accumulation at both sides of the interface implies a large amount of charge of opposite sign in a very small region. Such an amount of charges in this space must create a large increase in the recombination rate at the surface that can really affect charge collection at the TiO_2, thus worsen the performance of the cell. Next thing to include in the model is then the expected surface recombination.

For such an aim, we need to know the amount of charge at both sides of the interfaces, as well as its distribution and nature, since ionic charges will not affect directly to the recombination. To get to know this distribution, modelling of the band shape of both sides of the interface is needed. This implies calculating the electric potential by solving the Poisson equation for the electrons at the TiO_2 and for holes and ions at the perovskite and applying its continuity at the interface, as well as the continuity of the electric displacement field.

Here we show preliminary modelling and calculations carried out without the consideration of ions. Even without ions, we can estimate the size of the space-charge regions at both sides of the interface will be, as well as the amount of charge. An expression for the capacitance at both sides is also obtained and the resulting total capacitance calculated.

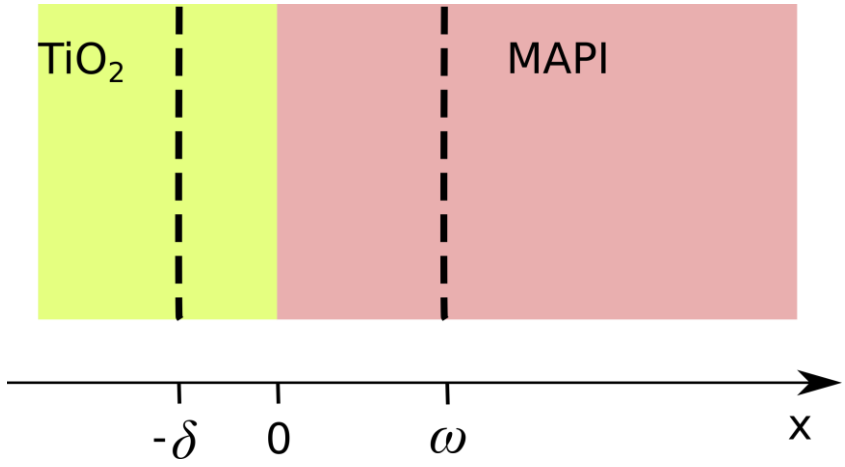

Fig. 6. Space-charge widths for both sides of the TiO_2-Perovskite interface.

In Fig. 6 I show the space charge regions for both the TiO_2 (δ) and the perovskite (w). Outside these two regions, bands at both sides become flat. In these flat regions, the electric field is null and the potential is constant, so the solution of the Poisson equation there is trivial.

Inside these regions, we must solve the Poisson equation to describe the curvature of the bands,

$$\frac{d^2\varphi}{dx^2} = -\frac{\rho(x)}{\varepsilon} \tag{13}$$

where φ is the electric potential, ρ the density of charge and ε the dielectric constant of the semiconductor.

Then, in the TiO_2 side, i.e. from $x = -\delta$ to $x = 0$, being an n-type semiconductor, one can neglect the minority carrier and the charge density is[38]

$$\rho(x) = q\left[N_D - n(x)\right] \tag{14}$$

with N_D being the density of donors and n the density of electrons. Here n is

$$n(x) = N_D \exp\left[\frac{q}{k_B T}\varphi(x)\right] \tag{15}$$

and the charge density is then

$$\rho(x) = qN_D\left[1 - \exp\left(\frac{q}{k_B T}\varphi(x)\right)\right] \tag{16}$$

Making the same considerations for the perovskite side, which goes from $x = 0$ to $x = w$, the charge density there is

$$\rho(x) = -qN_A\left[1 - \exp\left(\frac{q}{k_B T}\varphi(x)\right)\right] \tag{17}$$

When considering a potential large than thermal voltage, i.e. $\varphi(x) >> q/(k_B T)$, one can neglect part of the equation and consider the charge density as follows

$$\rho(x) = \begin{cases} -qN_D \exp\left(\dfrac{q}{k_B T}\varphi(x)\right) & -\delta < x < 0 \\ qN_A \exp\left(\dfrac{q}{k_B T}\varphi(x)\right) & 0 < x < \omega \end{cases} \tag{18}$$

With this, one can start solving Poisson equation at both sides, but with the following boundary conditions taken into account. First, the continuity of the electric potential must hold at the interface

$$\varphi(0^-) = \varphi(0^+) \tag{19}$$

Second, the difference between both potentials in the bulk regions, i.e. in $x < -\delta$ and $x > \omega$, is

$$\varphi(-\delta) - \varphi(w) = V - V_{bi} \tag{20}$$

As one has to solve a second order differential equation, the boundary conditions apply also for the first derivative of the potential, i.e. for the electric field. As said before, the field in the bulk is 0:

$$E(-\delta) = -\frac{\partial \varphi}{\partial x}_{x=-\delta} = 0, \quad E(w) = -\frac{\partial \varphi}{\partial x}_{x=\omega} = 0 \tag{21}$$

Finally, to get a full solution, the continuity of the electric displacement field D must also hold at the interface:

$$D(0^-) = \varepsilon_1 \frac{\partial \varphi}{\partial x}_{x=0^-} = \varepsilon_2 \frac{\partial \varphi}{\partial x}_{x=0^+} = D(0^+) \tag{22}$$

where ε_1 and ε_2 are the dielectric constants of the TiO_2 and the perovskite, respectively.

The final solution, for the potential at both sides, with the extrinsic Debye lengths

$$\begin{aligned} L_{D1} &= \sqrt{\frac{\varepsilon_1 k_B T}{N_D q^2}} \\ L_{D2} &= \sqrt{\frac{\varepsilon_2 k_B T}{N_A q^2}} \end{aligned} \tag{23}$$

is as follows for the TiO_2:

$$\varphi(x) = \varphi(-\delta) - \frac{2k_B T}{q} \ln\left[\sqrt{\frac{\varepsilon_1 L_{D2}}{\varepsilon_2 L_{D1}}} \exp\left(\frac{q}{4k_B T}(V_{bi} - V) \right) - \frac{x}{\sqrt{2} L_{D1}} \right] \tag{24}$$

and for the perovskite:

$$\varphi(x) = \varphi(\omega) + \frac{2k_B T}{q} \ln\left[\sqrt{\frac{\varepsilon_2 L_{D1}}{\varepsilon_1 L_{D2}}} \exp\left(\frac{q}{4k_B T}(V_{bi} - V) \right) + \frac{x}{\sqrt{2} L_{D2}} \right] \tag{25}$$

The width of the space-charge regions δ and ω are also calculated in terms of the applied voltage V:

$$\delta = \sqrt{2}L_{D1} - \sqrt{\frac{2\varepsilon_1 L_{D1} L_{D2}}{\varepsilon_2}} \exp\left[\frac{q}{4k_B T}(V_{bi} - V)\right] \tag{26}$$

and

$$\omega = \sqrt{2}L_{D2} - \sqrt{\frac{2\varepsilon_2 L_{D1} L_{D2}}{\varepsilon_1}} \exp\left[\frac{q}{4k_B T}(V_{bi} - V)\right] \tag{27}$$

With this overall solution, it is possible to simulate the shape of the bands and to calculate the width of the bands. In Fig. 7 the bands are shown for the case of accumulation at $V = V_{OC} = 1.15\,\mathrm{V}$. At this point, the accumulation is large enough to cross the Fermi Level in the perovskite, so the amount of charge there is enormous. Here, the values of the density of donors in the TiO_2 and acceptors in the perovskite are $N_{D1} = 6.2\times10^{18}\ \mathrm{cm}^{-3}$ and $N_{A2} = 1.8\times10^{17}\ \mathrm{cm}^{-3}$, respectively. The values of the dielectric constants are $\varepsilon_1 = 20\varepsilon_0$ and $\varepsilon_2 = 26\varepsilon_0$. The value of the built-in voltage here is $V = 0.7V$.

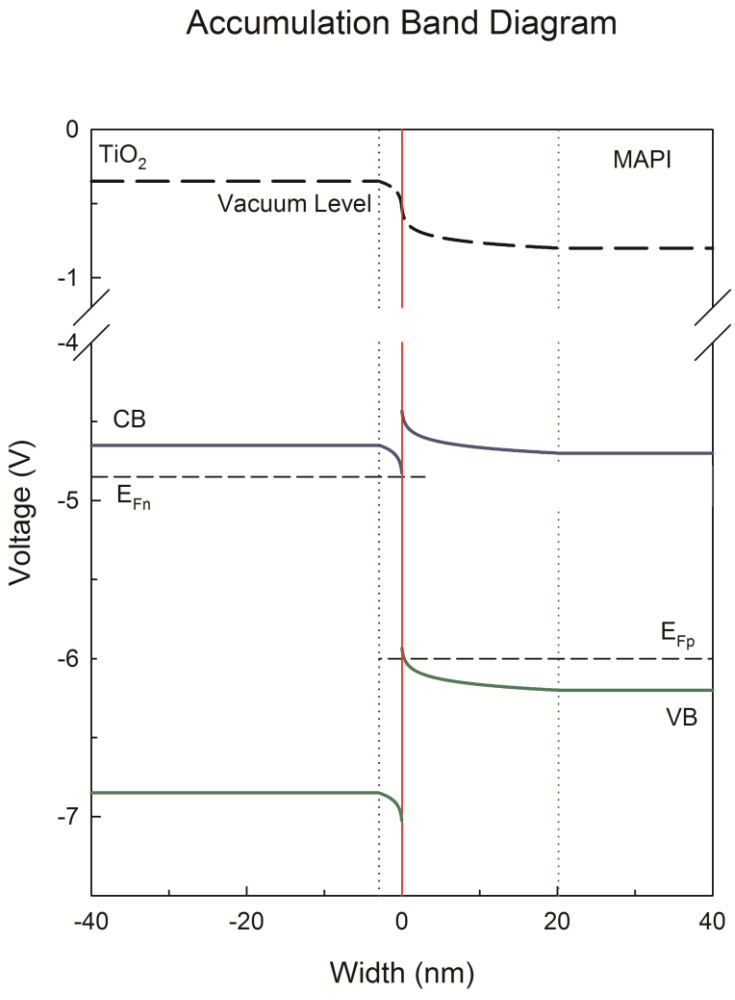

Fig. 7. Band diagram for the TiO_2-Perovskite interface.

When calculating the widths of the space-charge regions, we obtain $\delta = 2.9nm$ and $\omega = 20.2\,\mathrm{nm}$, which is in agreement of one would expect, since accumulation layers are really small.

From the expressions of the potentials it is possible to calculate the total charge space-charge region by Gauss law. The total charge is given by:

$$Q_{sc} = \varepsilon \frac{\partial \varphi}{\partial x}_{x=0} \tag{28}$$

And from with the total charge one obtains the accumulation capacitance[39] using:

$$C_{acc} = \varepsilon \frac{\partial Q_{sc}}{\partial \varphi(0)} \tag{29}$$

Then, the expression for both accumulation capacitances is given by

$$C_{acc} = \sqrt{\frac{\varepsilon_1 \varepsilon_2}{2L_{D1}L_{D2}}} \exp\left[\frac{q}{4k_B T}(V - V_{bi})\right] \tag{30}$$

And the value obtained for the accumulation capacitance is $C_{acc} = 205\,\mu\mathrm{F\,cm^{-2}}$ which is consistent with the values obtained in Table 1, as those are specially big, because those samples forced more than one injection layer and then, more accumulation layers. Then, this accumulation heterojunction model is a good start point for further calculations in which ions will be included.

6. Conclusions

The surface polarization model for the hysteresis in the perovskite solar cells previously developed has been here taken as a starting point. This model explains some types of hysteresis observed in perovskites j-V curves taking into consideration many of the proofs that have been reported for the accumulation of charge in the TiO_2-perovskite interface. The model assumes a surface voltage when going to forward bias above built-in voltage. This voltage has a slow kinetic discharge linked to ion slow motion. This voltage has an accumulation capacitance also linked with it.

To provide support to this model, it is taken here in another commonly used technique to characterize solar cells, the Impedance Spectroscopy. First, the IS model is calculated obtaining an inductive element many times observed in the experiments. The simulations made with the model correspond with two of the main features reported: on

one hand, two arcs that evolve in concordance, on the other hand, two exotic and unique behaviors of the perovskite, the inductive loops and the negative capacitances. The inductive loop and negative capacitances are obtained for the first time from pure calculation from the model. For further proof, two examples of this unique behaviors reported in the literature are taken here two fit them with the model. The values obtained for the parameters of the model are satisfactory, but there is not a fully concordance between the model and the real spectra. Further development of the model is needed.

The large accumulation assumed in the model should induce a big surface recombination due to the huge density of carriers in this interface. Therefore, the next step in the development of the model is to include this surface recombination. To such an aim, it is necessary to know how the distribution of charge will look like at both sides of the interface. Here, a preliminary model for the interface is calculated only including majority carriers, i.e. without the consideration of ions. Nevertheless, this heterojunction model for the accumulation already gives good values for the distribution of charge and the accumulation capacitance, so it is a good start point for the surface recombination.

References

1. *World energy resources 2016*. World Energy Council: UK, 2016.

2. Friedlingstein, P.; Houghton, R. A.; Marland, G.; Hackler, J.; Boden, T. A.; Conway, T. J.; Canadell, J. G.; Raupach, M. R.; Ciais, P.; Le Quere, C. Update on CO_2 emissions. *Nat. Geosci.* **2010,** *3*, 811-812.

3. Hernández, L. El problema energético en el desarrollo global y la energía fotovoltaica. *Rev. iberoam. física* **2006,** *2*, 5.

4. Tsoutsos, T.; Frantzeskaki, N.; Gekas, V. Environmental impacts from the solar energy technologies. *Energy Pol.* **2005,** *33*, 289-296.

5. Chapin, D. M.; Fuller, C. S.; Pearson, G. L. A new silicon p-n junction photocell for converting solar radiation into electrical power. *J. App. Phys.* **1954,** *25*, 676-677.

6. Rekinger, M.; Thies, F.; Masson, G.; Orlandi, S. *Global market outlook for photovoltaics 2015–2019.* European Photovoltaic Industry Association: Brussels **2015**.

7. Romeo, A. Development of thin-film Cu (In, Ga) Se_2 and CdTe solar cells. *Prog. Photovoltaics* **2004,** *12*, 93-111.

8. Grätzel, M. Dye-sensitized solar cells. *J. Photoch. Photobio. C* **2003,** *4*, 145-153.

9. Hoppe, H.; Sariciftci, N. S. Organic solar cells: an overview. *J Mater. Res.* **2004,** *19*, 1924-1945.

10. Yang, W. S.; Noh, J. H.; Jeon, N. J.; Kim, Y. C.; Ryu, S.; Seo, J.; Seok, S. I. High-performance photovoltaic perovskite layers fabricated through intramolecular exchange. *Science* **2015,** *348*, 1234.

11. Green, M. A.; Ho-Baillie, A.; Snaith, H. J. The emergence of perovskite solar cells. *Nat. Photonics* **2014,** *8*, 506-514.

12. Gonzalez-Pedro, V.; Juarez-Perez, E. J.; Arsyad, W.-S.; Barea, E. M.; Fabregat-Santiago, F.; Mora-Sero, I.; Bisquert, J. General working principles of $CH_3NH_3PbX_3$ perovskite solar cells. *Nano Lett.* **2014,** *14*, 888–893.

13. Todinova, A.; Idígoras, J.; Salado, M.; Kazim, S.; Anta, J. A. Universal features of electron dynamics in solar cells with TiO_2 contact: from dye solar cells to perovskite solar cells. *J. Phys. Chem. Lett.* **2015,** *6*, 3923-3930.

14. Pascoe, A. R.; Duffy, N. W.; Scully, A. D.; Huang, F.; Cheng, Y.-B. Insights into planar $CH_3NH_3PbI_3$ perovskite solar cells using impedance spectroscopy. *J. Phys. Chem. C* **2015,** *119*, 4444–4453.

15. Pockett, A.; Eperon, G. E.; Peltola, T.; Snaith, H. J.; Walker, A. B.; Peter, L. M.; Cameron, P. J. Characterization of planar lead halide perovskite solar cells by impedance spectroscopy, open circuit photovoltage decay and intensity-modulated

photovoltage/photocurrent spectroscopy. *J. Phys. Chem. C* **2015,** *119*, 3456–3465.

16. Guerrero, A.; Garcia-Belmonte, G.; Mora-Sero, I.; Bisquert, J.; Kang, Y. S.; Jacobsson, T. J.; Correa-Baena, J.-P.; Hagfeldt, A. Properties of contact and bulk impedances in hybrid lead halide perovskite solar cells including inductive loop elements. *J. Phys. Chem. C* **2016,** *120*, 8023-8032.

17. Bisquert, J.; Garcia-Belmonte, G.; Guerrero, A. Impedance characteristics of hybrid organometal halide perovskite solar cells. In *Organic-inorganic halide perovskite photovoltaics: from fundamentals to device architectures*, Park, N.-G.; Grätzel, M.; Miyasaka, T., Eds. Springer: 2016.

18. Almora, O.; Guerrero, A.; Garcia-Belmonte, G. Ionic charging by local imbalance at interfaces in hybrid lead halide perovskites. *Appl. Phys. Lett.* **2016,** *108*, 043903.

19. Sanchez, R. S.; Gonzalez-Pedro, V.; Lee, J.-W.; Park, N.-G.; Kang, Y. S.; Mora-Sero, I.; Bisquert, J. Slow dynamic processes in lead halide perovskite solar cells. Characteristic times and hysteresis. *J. Phys. Chem. Lett.* **2014,** *5*, 2357−2363.

20. Zohar, A.; Kedem, N.; Levine, I.; Zohar, D.; Vilan, A.; Ehre, D.; Hodes, G.; Cahen, D. Impedance spectroscopic indication for solid state electrochemical Reaction in $(CH_3NH_3)PbI_3$ films. *J. Phys. Chem. Lett.* **2016,** *7*, 191-197.

21. Anaya, M.; Zhang, W.; Hames, B. C.; Li, Y.; Fabregat-Santiago, F.; Calvo, M. E.; Snaith, H. J.; Miguez, H.; Mora-Sero, I. Electron injection and scaffold effects in perovskite solar cells. *J. Mater. Chem. C* **2017,** *5*, 634-644.

22. Mora-Seró, I.; Bisquert, J.; Fabregat-Santiago, F.; Garcia-Belmonte, G.; Zoppi, G.; Durose, K.; Proskuryakov, Y. Y.; Oja, I.; Belaidi, A.; Dittrich, T.; Tena-Zaera, R.; Katty, A.; Lévy-Clement, C.; Barrioz, V.; Irvine, S. J. C. Implications of the negative capacitance observed at forward bias in nanocomposite and polycrystalline solar cells. *Nano Lett.* **2006,** *6*, 640-650.

23. Ravishankar, S.; Almora, O.; Echeverría-Arrondo, C.; Ghahremanirad, E.; Aranda, C.; Guerrero, A.; Fabregat-Santiago, F.; Zaban, A.; Garcia-Belmonte, G.; Bisquert, J. Surface polarization model for the dynamic hysteresis of perovskite solar cells. *J. Phys. Chem. Lett*. **2017**, 915-921.

24. Snaith, H. J.; Abate, A.; Ball, J. M.; Eperon, G. E.; Leijtens, T.; Noel, N. K.; Stranks, S. D.; Wang, J. T.-W.; Wojciechowski, K.; Zhang, W. Anomalous hysteresis in perovskite solar cells. *J. Phys. Chem. Lett.* **2014,** *5*, 1511-1515.

25. Kim, H.-S.; Park, N.-G. Parameters affecting I–V hysteresis of CH3NH3PbI3 perovskite solar cells: effects of perovskite crystal size and mesoporous TiO_2 layer. *J. Phys. Chem. Lett.* **2014,** *5*, 2927-2934.

26. Nemnes, G. A.; Besleaga, C.; Tomulescu, A. G.; Pintilie, I.; Pintilie, L.; Torfason, K.; Manolescu, A. Dynamic electrical behavior of halide perovskite based solar cells. *Sol. Energ. Mat. Sol. C.* **2017,** *159*, 197-203.

27. Contreras, L.; Idigoras, J.; Todinova, A.; Salado, M.; Kazim, S.; Ahmad, S.;

Anta, J. A. Specific cation interactions as the cause of slow dynamics and hysteresis in dye and perovskite solar cells: a small-perturbation study. *Phys. Chem. Chem. Phys.* **2016,** *18*, 31033-31042.

28. Bergmann, V. W.; Guo, Y.; Tanaka, H.; Hermes, I. M.; Li, D.; Klasen, A.; Bretschneider, S. A.; Nakamura, E.; Berger, R.; Weber, S. A. L. Local time-dependent charging in a perovskite solar cell. *ACS Appl. Mater. Inter.* **2016,** *8*, 19402-19409.

29. Zarazua, I.; Bisquert, J.; Garcia-Belmonte, G. Light-induced space-charge accumulation zone as photovoltaic mechanism in perovskite solar cells. *J. Phys. Chem. Lett.* **2016,** *7*, 525-528.

30. Gottesman, R.; Lopez-Varo, P.; Gouda, L.; Jimenez-Tejada, J. A.; Hu, J.; Tirosh, S.; Zaban, A.; Bisquert, J. Dynamic phenomena at perovskite/electron-selective contact interface as interpreted from photovoltage decays. *Chem* **2016,** *1*, 776-789.

31. Almora, O.; Zarazua, I.; Mas-Marza, E.; Mora-Sero, I.; Bisquert, J.; Garcia-Belmonte, G. Capacitive dark currents, hysteresis, and electrode polarization in lead halide perovskite solar cells. *J. Phys. Chem. Lett.* **2015,** *6*, 1645-1652.

32. Almora, O.; Aranda, C.; Mas-Marzá, E.; Garcia-Belmonte, G. On Mott-Schottky analysis interpretation of capacitance measurements in organometal perovskite solar cells. *Appl. Phys. Lett.* **2016,** *109*, 173903.

33. Shao, Y.; Xiao, Z.; Bi, C.; Yuan, Y.; Huang, J. Origin and elimination of photocurrent hysteresis by fullerene passivation in $CH_3NH_3PbI_3$ planar heterojunction solar cells. *Nat. Commun.* **2014,** *5*, 5784.

34. Zarazua, I.; Han, G.; Boix, P. P.; Mhaisalkar, S.; Fabregat-Santiago, F.; Mora-Seró, I.; Bisquert, J.; Garcia-Belmonte, G. Surface recombination and collection efficiency in perovskite solar cells from impedance analysis. *J. Phys. Chem. Lett.* **2016,** *7*, 5105-5113.

35. Correa-Baena, J.-P.; Turren-Cruz, S.-H.; Tress, W.; Hagfeldt, A.; Aranda, C.; Shooshtari, L.; Bisquert, J.; Guerrero, A. Changes from bulk to surface recombination mechanisms between pristine and cycled perovskite solar cells. *ACS Energy Lett.* **2017**, 681-688.

36. Bisquert, J.; Garcia-Belmonte, G.; Mora-Sero, I. Characterization of capacitance, transport and recombination parameters in hybrid perovskite and organic solar cells. In *Unconventional thin film photovoltaics* Como, E. D.; Angelis, F. D.; Snaith, H.; Walker, A., Eds. Royal Society of Chemistry: 2016.

37. Chen, Y. F.; Tsai, Y. T.; Bassani, D. M.; Clerc, R.; Forgacs, D.; Bolink, H. J.; Wussler, M.; Jaegermann, W.; Wantz, G.; Hirsch, L. Evidence of band bending induced by hole trapping at $MAPbI_3$ perovskite/metal interface. *J. Mater. Chem. A* **2016,** *4*, 17529-17536.

38. Bisquert, J.; Garcia-Belmonte, G.; Fabregat-Santiago, F. Modelling the electric potential distribution in the dark in nanoporous semiconductor electrodes. *J. Solid State Electr.* **1999,** *3*, 337-347.

39. Bisquert, J. *Nanostructured energy devices : equilibrium concepts and kinetics*. CRC Press Taylor & Francis Group: Boca Raton, 2014.